scientific reports

Check for updates

OPEN

Comprehensive analysis of cuproptosis and m6A-Target gene signatures for diagnostic significance and immune microenvironment characterization in polycystic ovary syndrome

Yang Liu[1,2]✉, Yujie Gengxiao[1,2], Yanzhi Wu[1], Yan Li[1], Xi Hu[1] & Jia Bie[1]✉

Polycystic Ovary Syndrome (PCOS) lacks specific biomarkers for early diagnosis. Recent evidence implicates cuproptosis, a copper-induced regulated cell death pathway, and N6-methyladenosine (m6A) RNA modifications in metabolic and inflammatory processes central to PCOS pathogenesis. This study aimed to construct integrated diagnostic signatures based on cuproptosis- and m6A-related gene expression. Transcriptome data from GEO datasets (GSE95728, GSE106724, GSE114419) comprising 28 PCOS and 22 control granulosa cell samples were merged and batch-corrected. Differentially expressed genes (DEGs) overlapping with curated cuproptosis-related and m6A-target gene sets were identified. LASSO regression was applied to generate diagnostic models based on selected DEGs: *CASK*, *AGMAT*, *NEDD4*, and *PTGES3* (cuproptosis); *CLDN1*, *ACLY*, and *DDX3X* (m6A). The combined model achieved excellent diagnostic accuracy (AUC up to 0.960), validated in an independent dataset (GSE168404). ssGSEA analysis revealed immune dysregulation involving dendritic cells, T cell subsets, and myeloid-derived suppressor cells, which correlated with risk scores. Drug-gene association analysis via CellMiner indicated therapeutic relevance of targets such as *ACLY* and *CLDN1* (Vinblastine), as well as *CASK* and *CLDN1* (XAV-939). qRT-PCR validation in granulosa cells from 5 PCOS patients and 5 controls confirmed gene expression trends. These findings suggest cuproptosis- and m6A-based signatures may enable accurate PCOS diagnosis and guide individualized immunomodulatory strategies.

Keywords Polycystic ovary syndrome, Cuproptosis, M6A modification, Risk scores, Immune microenvironment, Biomarkers

Polycystic ovary syndrome (PCOS) is a prevalent endocrine disorder in reproductive-age women, characterized by irregular menstrual cycles, hyperandrogenism, and ovarian dysfunction[1]. With a global prevalence ranging from 5 to 20%, PCOS poses significant risks to reproductive health and contributes to metabolic disturbances, including insulin obesity, insulin resistance, and cardiovascular diseases[2,3]. Despite its high prevalence, diagnosis remains challenging due to its clinical heterogeneity and the absence of a definitive biomarker[4]. This complexity often delays timely intervention[5], highlighting the need for novel diagnostic markers and mechanistic insights.

Although PCOS is not a malignant condition, its ovarian microenvironment exhibits striking similarities to the tumor microenvironment (TME), including chronic inflammation, immune cell infiltration, and metabolic reprogramming[6]. These features suggest that molecular mechanisms classically associated with tumor biology, such as regulated cell death pathways and epigenetic remodeling, may also play key roles in PCOS pathogenesis. This conceptual parallel provides a rationale for exploring gene signatures involved in processes like cuproptosis and RNA methylation in the context of PCOS.

[1]Department of Reproductive Medicine, The Second Affiliated Hospital of Kunming Medical University, Kunming 650101, China. [2]Yang Liu and Yujie Gengxiao contributed equally. ✉email: 13518735544@163.com; 791630202@qq.com

Cuproptosis is a newly identified form of regulated cell death triggered by copper accumulation. It involves copper binding to lipoylated components of the tricarboxylic acid cycle, leading to protein aggregation, iron-sulfur cluster loss, and ultimately, proteotoxic stress-induced cell death[7]. Intriguingly, mitochondrial dysfunction, a hallmark of cuproptosis, has been observed in PCOS patients, including impaired oxygen consumption and elevated reactive oxygen species[8,9]. Given copper's role in mitochondrial enzymes and evidence suggesting that elevated copper levels negatively impact follicle development in PCOS[10,11], cuproptosis may contribute to the pathophysiology of PCOS. Indeed, cuproptosis-related genes have demonstrated diagnostic values in other diseases such as cancer and cardiovascular conditions[12,13], prompting exploration of their relevance in PCOS.

Epigenetic modifications, particularly N6-methyladenosine (m6A) RNA methylation, have emerged as key regulators of gene expression and post-transcriptional processes. m6A modifications are installed, removed, and interpreted by methyltransferases, demethylases, and m6A-binding proteins, respectively, and play critical roles in mRNA stability, splicing, translation, and cellular signaling[14]. Accumulating evidence implicates m6A regulatory machinery in granulosa cell proliferation and apoptosis in PCOS[15–17]. Moreover, the immune dysregulation and low-grade inflammation associated with PCOS[18–20] may be linked to both RNA methylation pathways and trace element metabolism such as copper. Notably, Ferredoxin 1, a critical cuproptosis regulator, has shown gene expression correlation with m6A-, m5C-, and m1A-related genes in PCOS, suggesting potential mechanistic overlap[21].

Other RNA modifications, such as N7-methylguanosine (m7G), and genes involved in copper metabolism have also been implicated in PCOS development and progression[22]. Furthermore, integrated analyses of m6A and cuproptosis-related gene signatures have successfully identified prognostic markers in cancer[23]. These precedents led us to hypothesize that m6A- and cuproptosis-associated gene expression signatures may provide new diagnostic insights into PCOS. Therefore, this study aimed to identify differentially expressed m6A-target and cuproptosis-related genes in PCOS, develop diagnostic models based on these signatures, and explore their association with the ovarian immune microenvironment.

Methods

Data acquisition

Transcriptome expression profile data were obtained from the Gene Expression Omnibus database (GEO; https://www.ncbi.nlm.nih.gov/geo/). The datasets include GSE34526, GSE137684, GSE80432, GSE114419, GSE102293, and GSE168404. Datasets GSE34526, GSE137684, GSE80432, GSE114419, and GSE102293 were integrated, comprising human granulosa cell samples isolated from 28 PCOS ovaries and 22 normal ovaries (Table 1). These merged datasets were utilized for biomarker identification and model development. GSE168404 was reserved for validation purposes. Probes from each dataset were mapped to their corresponding genes, and those not matching any known gene were excluded. When multiple probes mapped to the same gene, their median expression value was used to represent the gene's expression. Potential batch effects were removed across the merged datasets using the ComBat function from the "sva" R package, which uses an empirical Bayes framework to adjust for non-biological variation while preserving biological differences[24]. Principal Component Analysis (PCA) was performed before and after batch correction to visually confirm the effectiveness of ComBat-based adjustment. Genes associated with cuproptosis were identified by querying the GeneCards database with the term "Copper death". By filtering for "Protein Coding" genes, we obtained 2,265 cuproptosis-associated genes. A total of 701 m6A target genes were further identified by sourcing the experimentally validated genes from the human genome (hg38) available at the m6A2 Target database (http://rm2target.cancerics.org/#/home). An overview of the study design is illustrated in Fig. 1.

Identification of differentially expressed genes

Differentially expressed genes (DEGs) between the PCOS and normal groups were identified using the R package 'limma'. Genes were considered DEGs if they had a p-value of less than 0.05. DEGs that overlapped with the list of cuproptosis-associated genes were defined as cuproptosis-related DEGs, and those overlapping with the m6A target gene list were defined as m6A-target DEGs.

Enrichment analysis

Gene Ontology (GO) and Kyoto Encyclopedia of Genes and Genomes (KEGG) functional enrichment analyses were carried out on cuproptosis-related and m6A-target DEGs using the R package 'clusterProfiler'. The p-values

ID	Platform	Sample type	Sample size	Data types	Role in study
GSE34526	GPL570	Human granulosa cells (PCOS or Normal Ovaries)	10	mRNA array	Merged Dataset (Discovery)
GSE137684	GPL17077		12	mRNA array	
GSE80432	GPL6244		16	mRNA array	
GSE114419	GPL17586		6	mRNA array	
GSE102293	GPL570		6	mRNA array	
Total Merged	Multiple		50 (28 PCOS, 22 Control)	mRNA array	Model Development
GSE168404	GPL16791		10	RNAseq	Independent Validation Dataset

Table 1. Sample size and sample types.

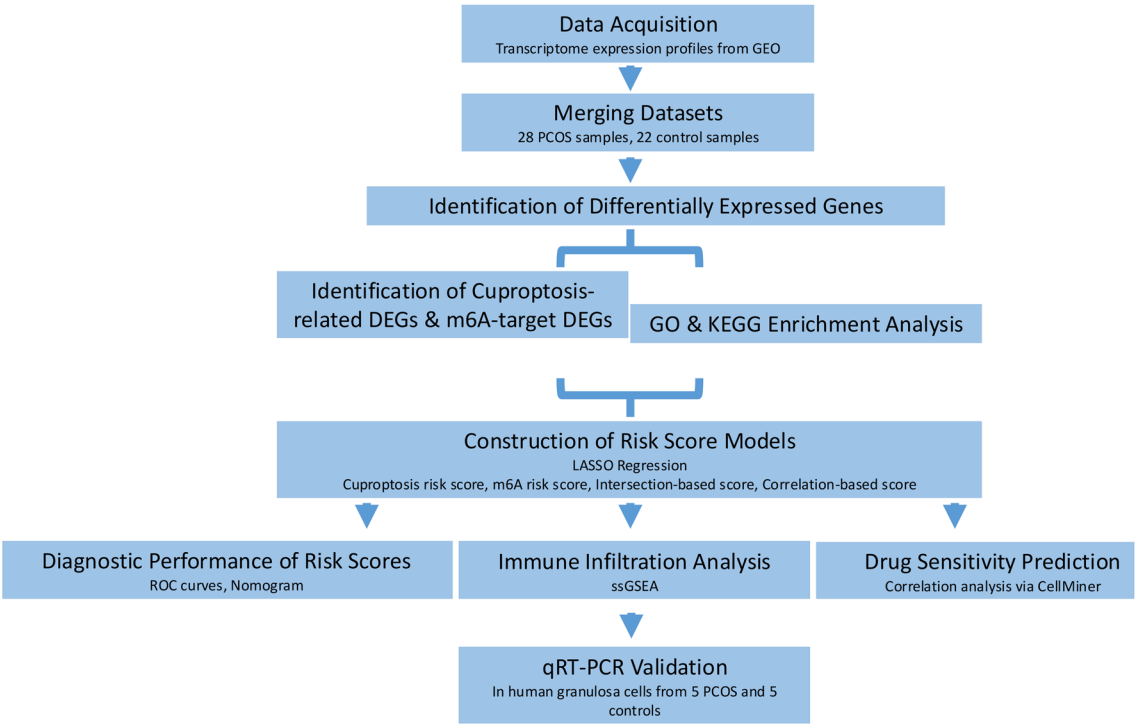

Fig. 1. Overview of the study design integrating bioinformatic analysis and experimental validation in Polycystic Ovary Syndrome (PCOS).

were adjusted using the Benjamini-Hochberg correction method, and the top 15 with the most significant adjusted *p*-values are presented.

Construction of the risk-scoring models

Cuproptosis-related and m6A-target DEGs were subjected to LASSO regression analysis using the R package "glmnet"[25]. The optimal penalty parameter (λ) was established based on the minimum criterion. Genes with non-zero coefficients were considered optimal variables. Weighted coefficients from the model, in conjunction with gene expression data, were used to compute the cuproptosis risk score and the m6A risk score. Comprehensive risk-scoring models were created using two approaches. One approach identified common genes between cuproptosis-related and m6A-target DEGs (intersection set), resulting in the intersection-based risk score. The other identified correlated genes between cuproptosis-related and m6A-target DEGs (correlation set) using Pearson correlation analysis. Key genes with $p < 0.001$ and |correlation coefficient| > 0.8 within this set were identified using a LASSO regression model to build the correlation-based risk score. The risk scores were calculated following this formula: Risk Score = $\sum$ (coefficient$_I$ × expression level$_I$), where expression level$_I$" is the normalized expression value of gene "I" and "coefficient$_I$" is its corresponding LASSO regression coefficient.

The diagnostic efficacy of the risk score in the merged and validation datasets was evaluated using Receiver Operating Characteristic (ROC) curve analysis with the R package "pROC"[26], calculating the Area Under the Curve (AUC). Additionally, patients were categorized into high and low-risk groups based on the median risk score using the "clusterProfiler" package[27]. A Gene Set Enrichment Analysis (GSEA) was then conducted on the GO functions and KEGG pathways for patients of varying risks.

Nomogram construction and evaluation

A diagnostic nomogram integrating cuproptosis risk score and m6A risk score was constructed using the R package "rms"[28]. The clinical decision-making performance of the nomogram was then assessed through calibration curves (using the "calibrate" function from the "rms" package) and Decision Curve Analysis (DCA) curves employing the "ggDCA" package[29].

Immune infiltration analysis

The enrichment scores of 28 immune cell subtypes were evaluated using single-sample gene set enrichment analysis (ssGSEA) as previously reported[30] using the "GSVA" package[31]. Immune cell abundance between PCOS and control groups was compared using the Wilcoxon rank-sum test. The relationship between the risk scores and immune cell infiltration was assessed using the Pearson correlation analysis.

Drug sensitivity prediction

The correlation between feature genes (genes included in the risk models) and drug sensitivity was investigated using the expression data of the NCI-60 cell line panel from the CellMiner database (https://discover.nci.nih.go

v/cellminer/home.do) and associated drug activity data. Correlation analysis between gene expression and drug IC50 values was performed using the Pearson method. The relationships between the feature genes and drugs were visualized.

Isolation and identification of human luteinized granulosa cells

Human luteinized granulosa cells were obtained from 5 PCOS patients and 5 age-matched infertile women with tubal factor infertility undergoing IVF/ICSI-ET. The study was approved by the Ethics Committee of the Second Affiliated Hospital of Kunming Medical University (No.2023 – 238). All participants provided written informed consent. We confirmed that all methods were performed in accordance with the relevant guidelines. All procedures were performed in accordance with the ethical standards laid down in the 1964 Declaration of Helsinki and its later amendments. The inclusion criteria for the PCOS group were as follows: (1) individuals who underwent IVF/ICSI-ET assisted reproductive treatment at the Department of Reproductive Medicine, the Second Affiliated Hospital of Kunming Medical University; (2) individuals less than 35 years old; (3) individuals meeting at least two of the 2003 Rotterdam Polycystic Ovary Syndrome PCOS diagnostic criteria or the 2018 Chinese PCOS diagnostic criteria[32,33], including irregular ovulation, hyperandrogenism or related clinical manifestations, and polycystic ovarian changes as detected by ultrasound (more than 12 small follicles with a diameter of 2–9 mm on both sides of the ovary, or an increased ovarian volume defined as greater than 10 mL). Exclusion criteria included other reproductive system diseases, immune diseases, medical conditions impacting pregnancy, chromosomal abnormalities, and diabetes. The inclusion criteria for the control group were individuals who received IVF-ET/ICSI assisted pregnancy treatment due to male factors or fallopian tube factors, utilized egg growth or antagonist programs to promote ovulation, were less than 35 years old, had basal follicle-stimulating hormone levels below 10 IU/L, and exhibited normal ovarian function (anti-Müllerian hormone greater than 1.1 ng/mL). The exclusion criteria were identical to those of the PCOS group.

Human luteinized granulosa cells were isolated and cultured using density gradient centrifugation. Following egg retrieval, follicular fluid was collected and centrifuged at 2000 rpm for 10 min to obtain granulosa cells, which were then resuspended in the medium and layered onto Ficoll solution (Solarbio, China) before centrifugation. The granulosa cell layer was collected, washed, and cultured in Petri dishes or plates with regular medium changes. Immunofluorescence was employed for cell identification. Cells were fixed, permeabilized, and blocked before incubation with primary antibodies against follicle-stimulating hormone receptor (FSHR; Abcam, Cambridge, UK) and subsequent secondary antibodies. Finally, cells were visualized under a confocal microscope. FSHR is a well-established marker for granulosa cells, particularly in the context of IVF protocols where luteinization is induced, although its expression levels can vary. The morphological characteristics and the isolation procedure itself further support the identity of the isolated cells as luteinized granulosa cells.

qRT-PCR

Total RNA was isolated from human luteinized granulosa cells using TRIzol. Reverse transcription was performed using a SweScript first-strand cDNA synthesis kit (Servicebio, Wuhan, China), followed by PCR amplification using 2× Universal Blue SYBR Green qPCR Master Mix (Servicebio, Wuhan, China) on a CFX96 real-time PCR detection system (Bio-Rad, USA). GAPDH was used as an internal reference. The PCR primer sequences (5'–3') are summarized in Table 2. Each reaction was performed in triplicate. The relative gene expression was calculated using the $2^{-\Delta\Delta Ct}$ method.

Statistical analysis

All statistical analyses were performed using R (v4.3.0). The R packages "FactoMineR" and "factoextra" were employed for PCA and its visualization. Heatmaps were visualized using the "pheatmap" package. Venn

Gene	Forward primer	Reverse primer
GAPDH	TGACTTCAACAGCGACACCCA	CACCCTGTTGCTGTAGCCAAA
CASK	TGGAAGCTCTACGCTACTGC	GTTTAACAGGTGCCGAGTTTTC
AGMAT	CTTGTCGAAGTTTCACCACCGTA	CTTTGGGGAGAGCACATAGCATC
NEDD4	TTCCAATGATCTAGGGCCTTTAC	GAGGATCTTCCCATTGTGTTCT
PTGES3	CAAATGATTCCAAGCATAAAAGAAC	GGTAAATCTACATCCTCATCACCAC
CLDN1	CCTCCTGGGAGTGATAGCAAT	GGCAACTAAAATAGCCAGACCT
ACLY	ATCGGTTCAAGTATGCTCGGG	GACCAAGTTTTCCACGACGTT
DDX3X	ACGAGAGAGTTGGCAGTACAG	ATAAACCACGCAAGGACGAAC
BNIP3	CAGGGCTCCTGGGTAGAACT	CTACTCCGTCCAGACTCATGC
BCL2	GGTGGGGTCATGTGTGTGG	CGGTTCAGGTACTCAGTCATCC
MDM2	CAGTAGCAGTGAATCTACAGGGA	CTGATCCAACCAATCACCTGAAT
PIK3R1	AGCAACCTGGCAGAATTACG	GCTGCTGGAATGACAGGATT
COX5 A	ATCCAGTCAGTTCGCTGCTAT	CCAGGCATCTATATCTGGCTTG
VIM	AGTCCACTGAGTACCGGAGAC	CATTTCACGCATCTGGCGTTC
SORL1	CAAGGTGTACGGACAGGTTAGT	CCAATGCCAGGCTATCTCG

Table 2. qRT-PCR primers.

diagrams were created with the "ggvenn" package, and ROC curves were visualized using the "pROC" package. Unless specified otherwise, result plots were generated using either ggplot2 or the base R plot function. The Pearson method was applied for correlation analyses. The Wilcoxon rank-sum test was used to assess differences between two groups (e.g., gene expression, immune scores). A result was considered statistically significant with $p < 0.05$. Sample size calculations for the qRT-PCR validation were performed using G*Power software (v3.1) based on preliminary effect size estimates from transcriptomic data, targeting a power of > 0.8 and a significance level of 0.05. The calculation indicated that at least 25 samples per group were required. Our study included 5 PCOS patients and 5 controls for qRT-PCR validation, which exceeded the required sample size, ensuring sufficient power to detect differential gene expression. The Wilcoxon test was used to assess differences between two groups. A result was considered statistically significant with $p < 0.05$.

Results

Identification of DEGs between PCOS and control groups

To identify DEGs that distinguish PCOS from healthy controls, we collected gene expression data from five datasets: GSE34526, GSE137684, GSE80432, GSE114419, and GSE102293. The merged datasets included 28 PCOS samples and 22 control samples. Initial clustering patterns varied among different datasets (Fig. 2A and B), which were later resolved through batch effect removal. After this correction, samples exhibited consistent clustering (Fig. 2C and D). Applying a significance threshold of p-value < 0.05, 1179 DEGs were identified, with 520 upregulated genes and 659 downregulated genes (Fig. 2E, Table S1). The heatmap in Fig. 2F displays the top 20 DEGs.

Identification and functional enrichment analysis of cuproptosis-related DEGs and m6A-target DEGs

Then, we intersected the DEGs with genes associated with cuproptosis and m6A modifications. Initially, we attempted to find an intersection between DEGs and m6A regulatory genes. However, in the absence of overlap, we shifted our focus to the intersection with m6A-target genes. Cuproptosis-related DEGs comprised 102 upregulated and 119 downregulated genes (Fig. 2G). In contrast, m6A-target DEGs included 39 upregulated and 24 downregulated genes (Fig. 2H). Functional exploration was conducted via GO and KEGG enrichment analyses. Cuproptosis-related DEGs enriched biological processes (BP) included positive regulation of cytokine production, response to lipopolysaccharide, and response to molecules of bacterial origin. Noteworthy cellular components (CC) encompassed the secretory granule membrane, secretory granule lumen, and cytoplasmic vesicle lumen. Molecular functions (MF) embraced pattern recognition receptor activity, Toll-like receptor binding, and mannosyltransferase activity (Fig. S1A, Table S2). KEGG pathways highlighted C-type lectin receptor signaling pathway, lipid and atherosclerosis, legionellosis, Epstein-Barr virus infection, and apoptosis (Fig. S1B, Table S3).

For m6A-target DEGs, significant BP included the intrinsic apoptotic signaling pathway, viral process, and cytokine-mediated signaling pathway. Predominant CC were cytoplasmic stress granule, mitochondrial outer membrane, and organelle outer membrane.

However, there was no significant enrichment observed in MF (Fig. S1C, Table S4). The principal KEGG pathways were Epstein-Barr virus infection, PD-L1 expression and PD-1 checkpoint pathway in cancer, and apoptosis (Fig. S1D, Table S5).

Overlapping pathways between cuproptosis-related and m6A-target DEGs included intrinsic apoptotic signaling pathway, cytokine-mediated signaling pathway, cellular response to biotic stimulus, and extrinsic apoptotic signaling pathway. Furthermore, shared KEGG pathways encompassed C-type lectin receptor signaling pathway, lipid and atherosclerosis, apoptosis, NF-kappa B signaling pathway, and HIF-1 signaling pathway. These data indicate that genes associated with cuproptosis and m6A modifications display differential expression and potential intersections in specific biological pathways tied to immune responses, lipid metabolism, and apoptosis.

Construction of cuproptosis and m6A scoring models

To identify feature genes for predictive scoring models for PCOS, we employed LASSO regression analysis (Fig. 3A, B and D, and 3E). Among the cuproptosis-related DEGs, genes of significance were *CASK*, *AGMAT*, *NEDD4*, and *PTGES3*. Additionally, *CLDN1*, *ACLY*, and *DDX3X* were highlighted in the m6A-target DEGs. Risk score models, represented as cuproptosis risk score and m6A risk score, were derived using weight coefficients and gene expression levels from the LASSO models. The risk scores were calculated by multiplying each gene's normalized expression level by its corresponding LASSO coefficient:

cuproptosis risk score = (−0.845) × expression level of *CASK* + (−0.015) × expression level of *AGMAT* + (−0.294) × expression level of *NEDD4* + (−0.146) × expression level of *PTGES3*.

m6A risk score = (−0.297) × expression level of *CLDN1* + (−0.257) × expression level of *ACLY* + (0.182) × expression level of *DDX3X*.

ROC analysis revealed notable AUC values of 0.869 for cuproptosis risk score (Fig. 3C) and 0.810 for m6A risk score (Fig. 3F) within the merged datasets. Furthermore, in the validation dataset GSE168404, the AUC values were even more impressive at 0.920 for cuproptosis risk score and 0.960 for m6A risk score (Fig. 3G and H). The results suggest that these models possess significant predictive potential for PCOS.

Collaborative implications of cuproptosis and m6A risk scores in PCOS

To investigate the potential functional interactions between cuproptosis and m6A risk scores in PCOS, we divided the patients into high and low-risk groups using the median value of each risk score. The GSEA results indicated identical enrichment outcomes for both models (Fig. 4A and B), suggesting a collaborative functional

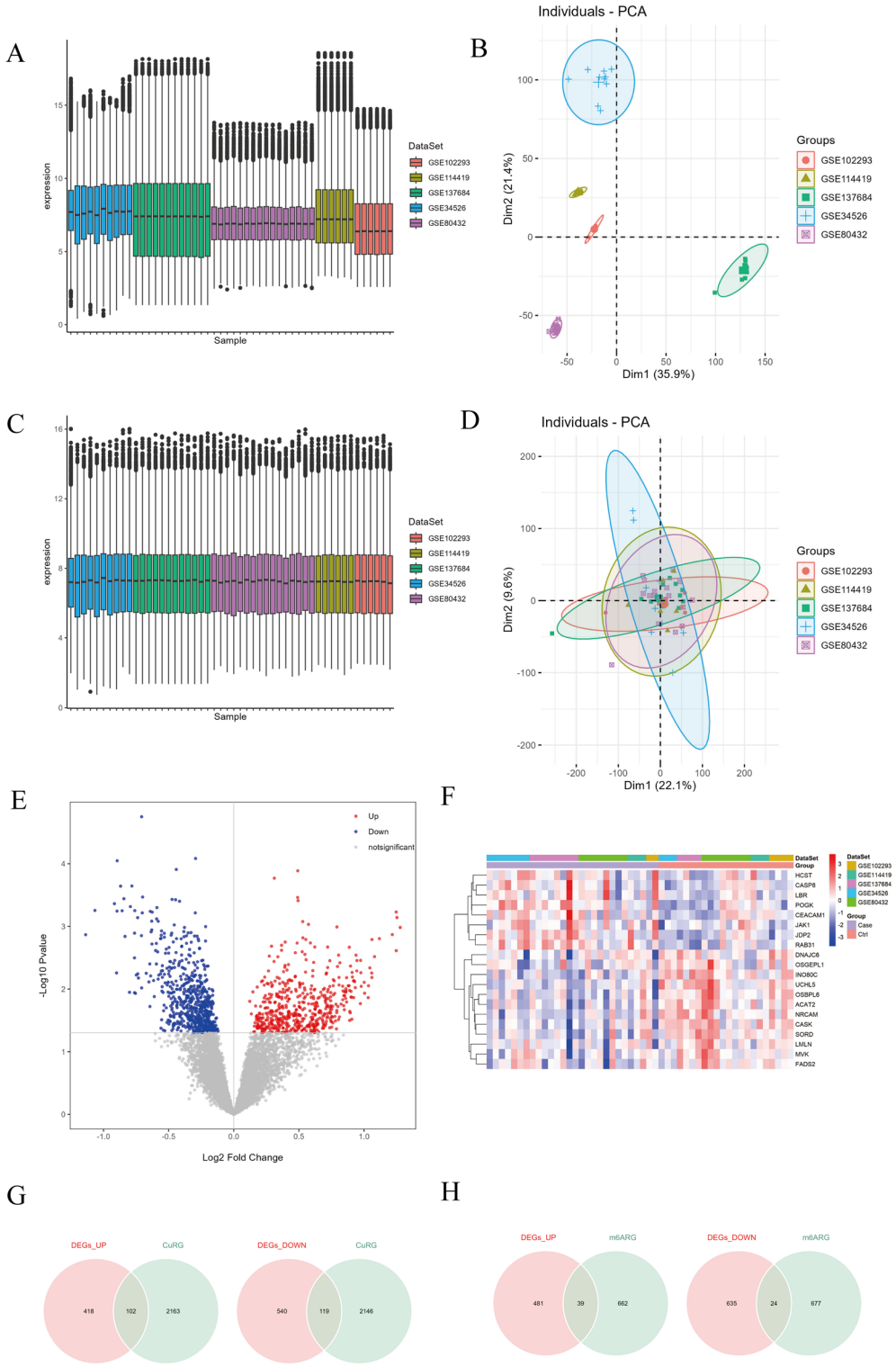

Fig. 2. Identification and characterization of differentially expressed genes (DEGs) between PCOS and control groups. (**A**, **B**) Box plots and Principal Component Analysis (PCA) before batch effect removal show significant heterogeneity among the five discovery datasets (GSE34526, GSE137684, GSE80432, GSE114419, GSE102293). (**C**, **D**) Box plots and PCA after ComBat batch effect removal demonstrate consistent expression patterns across the merged dataset (28 PCOS, 22 control samples). (**E**) Volcano plot illustrates 1179 DEGs ($p < 0.05$) between PCOS and control groups in the merged dataset (520 upregulated in red, 659 downregulated in blue). (**F**) Heatmap displays the expression of the top 20 DEGs (ranked by p-value). (**G**, **H**) Venn diagrams illustrate the intersection of total DEGs with cuproptosis-related genes to identify cuproptosis-related DEGs (**G**) and with m6A-target genes to identify m6A-target DEGs (**H**).

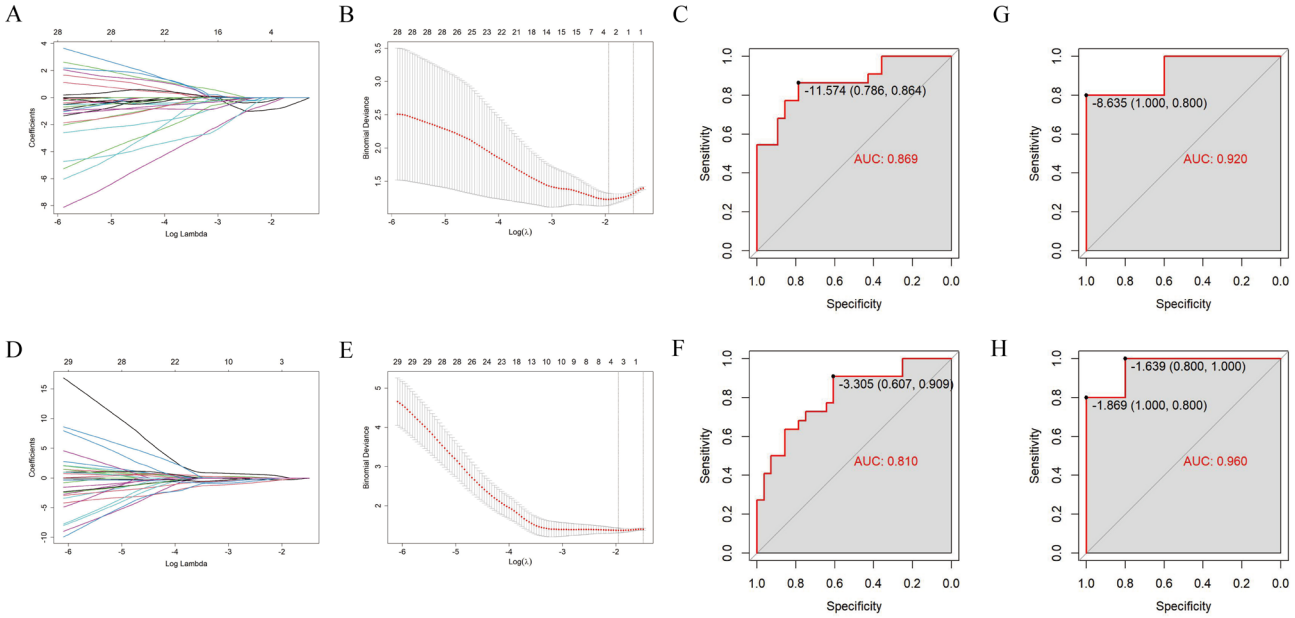

Fig. 3. Construction of cuproptosis and m6A risk-scoring models. (**A**, **D**) LASSO coefficient profiles for cuproptosis-related DEGs (**A**) and m6A-target DEGs (**D**). Coefficients are plotted against the log(λ) penalty parameter. (**B**, **E**) LASSO λ selection using minimum criteria. Vertical dotted lines indicate the optimal λ values chosen for the cuproptosis risk score model (**B**) and m6A risk score model (**E**). (**C**, **F**) ROC curves evaluating the diagnostic performance of cuproptosis risk score (**C**) and m6A risk score (**F**) for PCOS diagnosis in the merged discovery dataset. (**G**, **H**) ROC curves evaluating the diagnostic performance of cuproptosis risk score (**G**) and m6A risk score (**H**) in the independent validation dataset GSE168404. AUC values are indicated.

interaction between the two risk scores in PCOS patients. Furthermore, in both merged and external datasets, cuproptosis and m6A risk scores were significantly elevated in the PCOS group compared to the control group (Fig. 4C and D). A positive correlation between the risk scores further underscored their consistent associations (Fig. 4E and F), suggesting a collaborative role in characterizing PCOS.

Integrating risk-scoring models based on the intersection and expression correlation between cuproptosis-related DEGs and m6A-target DEGs

Recognizing the collaborative role of cuproptosis and m6A risk scores in predicting PCOS, we developed comprehensive risk-scoring models through two different approaches: one based on the intersection of cuproptosis-related and m6A-target DEGs, and the other founded on their expression correlation. Among the genes common to both cuproptosis-related DEGs and m6A-target DEGs, a set of 27 genes were identified (Fig. S2A-B). Utilizing the expression profiles of these common genes, a LASSO regression model revealed 7 key genes: *BNIP3*, *BCL2*, *MDM2*, *DDX3X*, *PIK3R1*, *COX5 A*, and *VIM*. The intersection-based risk score was computed as follows: (−0.224) × Expression(*BNIP3*) +0.131 × Expression(*BCL2*) + (−0.099) × Expression(*MDM2*) +0.558 × Expression(*DDX3X*) +0.110 × Expression(*PIK3R1*) + (−1.003) × Expression(*COX5 A*) +0.005 × Expression(*VIM*). The intersection-based score demonstrated strong diagnostic performance with an AUC value of 0.812 in the merged dataset and 1.000 in the external dataset (Fig. S2E-F).

Additionally, using Pearson correlation analysis for cuproptosis-related DEGs and m6A-target DEGs with criteria $p < 0.001$ and |correlation efficient| > 0.8, we identified 168 significantly correlated genes (Fig. S2C-D). Utilizing their expression profiles, we established another LASSO regression model and identified two critical genes, *CASK* and *SORL1*, both linked to cuproptosis. These two genes were selected based on having non-zero coefficients after applying LASSO regression to the expression data of the 168 correlated genes. The correlation-based risk score was calculated as (−1.314) × Expression(*CASK*) +0.001 × Expression(*SORL1*), yielding a diagnostic AUC value of 0.843 in the merged dataset and 0.920 in the external dataset (Fig. S2G-H). These integrated risk-scoring models provide valuable insights into the potential predictive power of the analyzed gene sets.

Diagnostic performance of risk scores in PCOS

To assess the diagnostic performance of cuproptosis risk score and m6A risk score in PCOS, we constructed a diagnostic nomogram. In the nomogram, the patient was scored according to the proportion of the regression coefficient for each risk score. By summing the corresponding scores (−1.54), we were able to predict a PCOS probability of 26.9% (Fig. 5A, S5). Calibration curves demonstrated the agreements between predicted probability and observed probability, suggesting the high predictive accuracy of the nomogram for PCOS (Fig. 5B). The DCA curve showed that the composite model provided greater clinical benefit than individual risk scores, highlighting its improved predictive performance and potential for enhanced clinical decision-making (Fig. 5C).

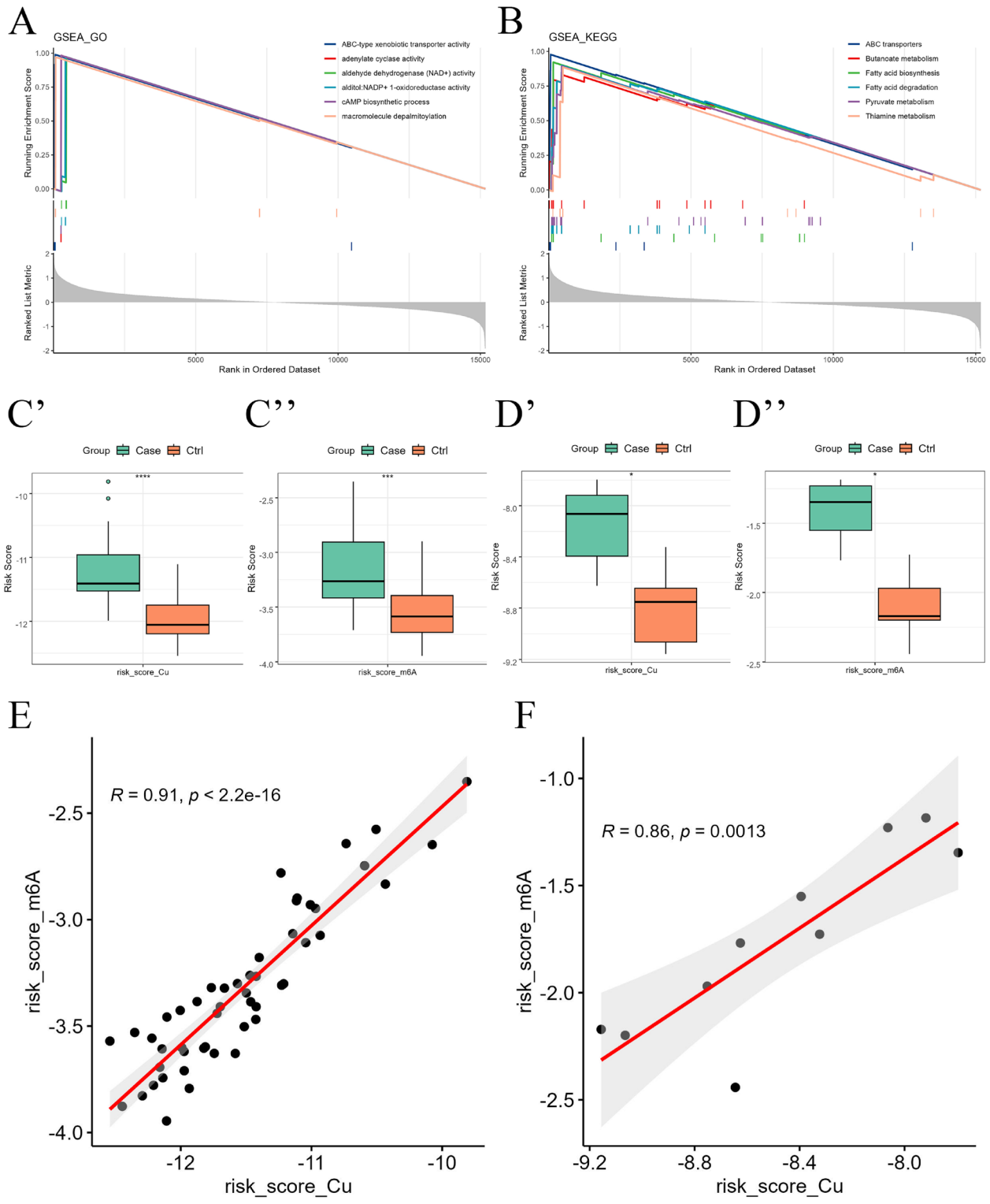

Fig. 4. Collaborative implications of cuproptosis risk score and m6A risk score in PCOS. (**A**, **B**) Gene Set Enrichment Analysis (GSEA) results showing representative enriched pathways for high-risk groups defined by median cuproptosis risk score (A) and m6A risk score (B). (**C**, **D**) [Revised] Box plots comparing cuproptosis risk score (**C**) and m6A risk score (**D**) between PCOS and control groups. These will be presented as separate plots due to different scales. Comparisons are shown for both the merged discovery dataset and the validation dataset GSE168404. Significance levels indicated (*$p < 0.05$, **$p < 0.01$). (**E**, **F**) Scatter plots showing the Pearson correlation between cuproptosis risk score and m6A risk score in the merged discovery dataset (**E**) and the validation dataset GSE168404 (**F**). Correlation coefficients (**R**) and p-values are shown.

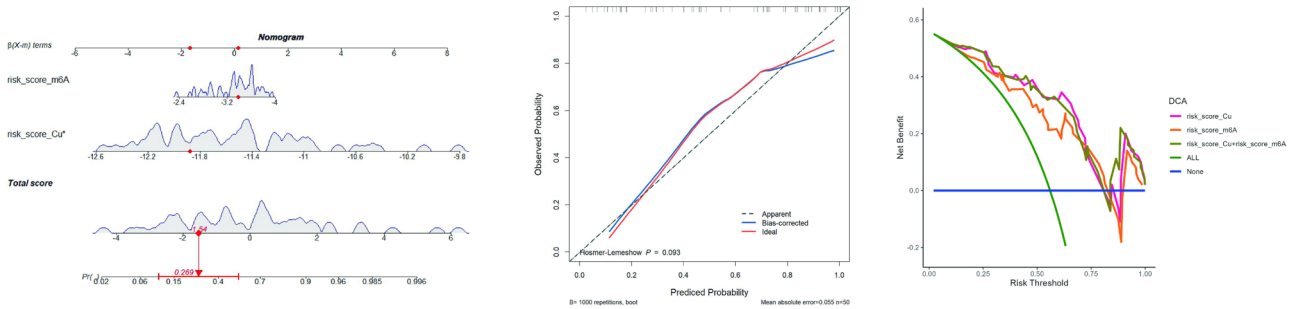

Fig. 5. Diagnostic performance of integrated risk scores in PCOS. (**A**) Nomogram integrating cuproptosis risk score and m6A risk score for predicting PCOS probability. Instructions: Locate patient scores on each risk score axis, draw lines upwards to the 'Points' axis, sum the points, and draw a line down from the 'Total Points' axis to the 'Probability of PCOS' axis. The example is shown (−1.54 total points corresponds to ~ 26.9% probability). (**B**) Calibration curve for the nomogram. The x-axis is the nomogram-predicted PCOS probability, the y-axis is the actual observed PCOS frequency. The diagonal dotted line represents perfect calibration. (**C**) Decision Curve Analysis (DCA) comparing the net benefit of using cuproptosis risk score alone, m6A risk score alone, or the combined nomogram model across a range of threshold probabilities for clinical decision-making.

Immune infiltration analysis

To understand the potential immunological associations and mechanisms underlying PCOS, we employed ssGSEA to analyze the differences in immune infiltration between PCOS and normal controls. A heatmap revealed a global trend toward heightened immune activity in PCOS, indicating a pro-inflammatory microenvironment (Fig. 6A). Although differences in individual cell types were observed (Fig. 6B), the overall pattern suggests broad immune dysregulation rather than changes confined to specific cell subsets. Notably, both the cuproptosis and m6A risk scores exhibited consistently positive correlations with multiple immune cell populations (Fig. 6C), supporting a shared link between these molecular signatures and enhanced immune activation in PCOS.

Correlation between feature genes and drug responses

To understand the connection between feature genes (genes included in cuproptosis risk score, m6A risk score, intersection-based risk score, correlation-based risk score) and drug responses, we acquired gene expression and drug sensitivity (IC50) data from the CellMiner database using the NCI-60 cell line panel. Clinical laboratory-tested and FDA standard-certified drugs underwent Pearson correlation analysis to establish associations between feature gene expression and drug sensitivity data. We selected gene-drug pairs with significant correlations based on criteria of $p < 0.05$ and |correlation coefficient| > 0.4 (Fig. 7, S6).

Remarkably, *ACLY* and *CLDN1* exhibited the strongest negative and positive correlations with Vinblastine, respectively, while *CLDN1* also demonstrated the most robust positive correlation with XAV-939. *AGMAT* displayed its most pronounced negative correlation with MTX-211 and a positive correlation with Barasertib, while *CASK* exhibited its strongest negative correlation with Dolastatin 10 and a positive correlation with XAV-939. Additionally, *DDX3X* displayed the strongest positive correlation with Methylprednisolone, and *PTGES3* demonstrated the most substantial negative correlation with AZD-3147 and a positive correlation with ST-3595. We also examined the correlation between intersection-based and correlation-based model genes and drug responses (Fig. S3, S6). The findings shed light on the potential role of these genes in guiding personalized treatment strategies for PCOS.

Validation of model gene alterations in clinical samples

To validate model gene dysregulation in clinical samples, we isolated human luteinized granulosa cells from 5 PCOS patients and 5 controls. Immunofluorescence analysis of FSHR demonstrated the successful isolation of the target cells (Fig. S4). The results of qRT-PCR showed that, compared to the control group, the expression of *AGMAT*, *CASK*, *CLDN1*, and *VIM* was significantly reduced in the PCOS group (all $p < 0.05$). Conversely, the expression of *BNIP3*, *DDX3X*, *ACLY*, *PIK3RI*, and *BCL2* was significantly increased in the PCOS group (all $p < 0.05$) (Fig. 8). These data were generally consistent with the bioinformatics analysis, suggesting that the dysregulation of these genes play a significant role in the pathogenesis of PCOS.

Discussion

In this study, we comprehensively analyzed cuproptosis-related DEGs and m6A-target DEGs for PCOS diagnosis. We developed and validated novel risk-scoring models based on these signatures, demonstrating robust diagnostic potential (AUC up to 0.960 in validation). Importantly, our study is among the first to integrate both cuproptosis and m6A modification pathways in PCOS diagnostics, revealing their synergistic potential[34,35]. Our findings align with previous studies showing correlations between these pathways in other diseases like hepatocellular carcinoma and breast cancer[36,37], highlighting the novelty of applying this combined approach to PCOS.

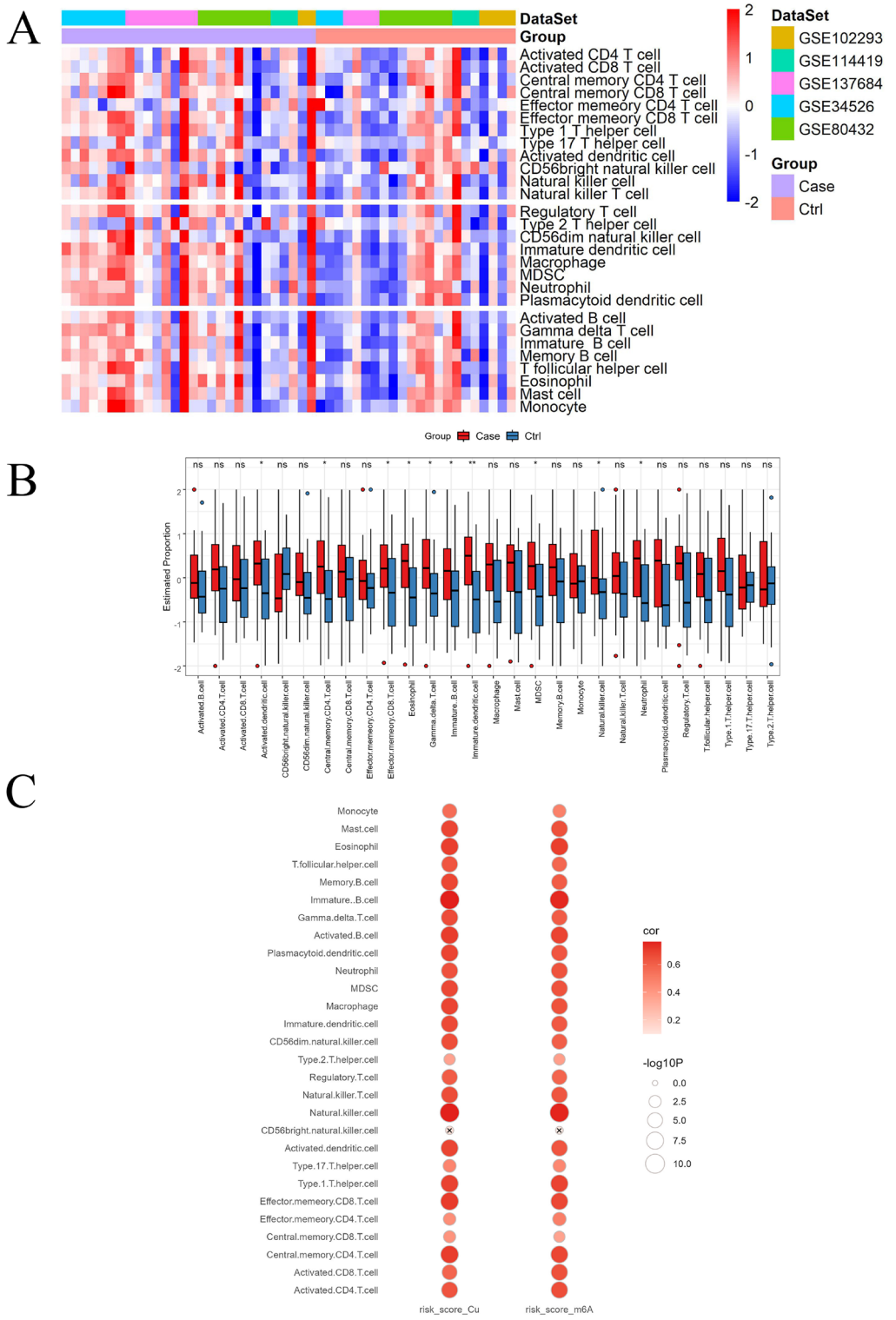

Fig. 6. Immune infiltration analysis. (**A**) Heatmap illustrating the ssGSEA enrichment scores for 28 immune cell types across PCOS and control samples in the merged dataset. (**B**) Box plots comparing the enrichment scores of significantly different immune cell types between PCOS and control groups (Wilcoxon test, $^{*}p < 0.05$, $^{**}p < 0.01$). (**C**) Correlation plot showing Pearson correlation coefficients between immune cell enrichment scores and the cuproptosis and m6A risk scores. The intensity of the red color is proportional to the positive correlation coefficient value. The size of the circle indicates statistical significance (larger circles denote greater significance/smaller P-values). Non-significant correlations are marked with '×'.

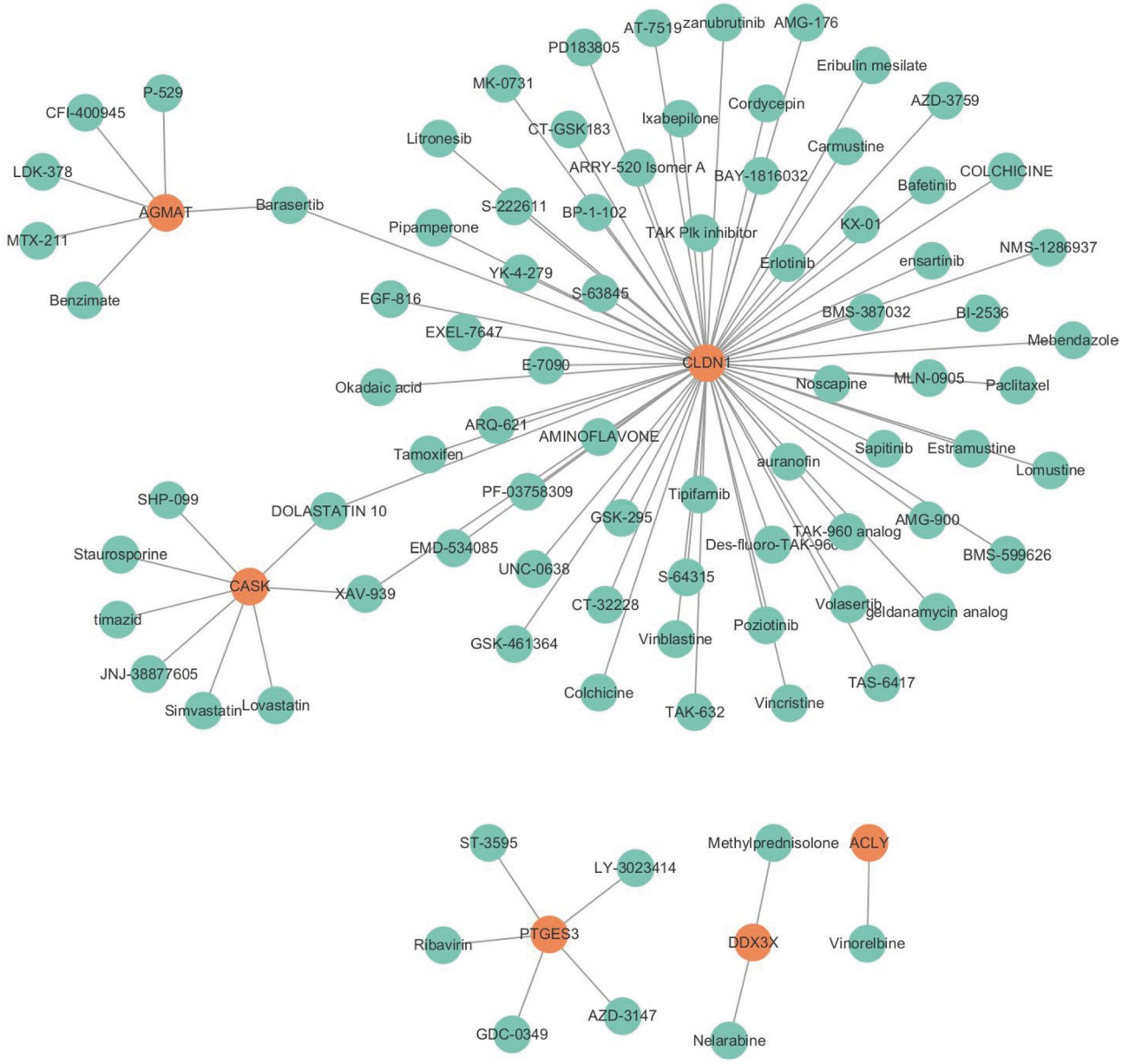

Fig. 7. Correlation between feature genes and drug responses. Orange indicates feature genes, and green indicates drugs significantly correlated with the feature genes.

The individual genes identified in our primary signatures (cuproptosis risk model: *CASK*, *AGMAT*, *NEDD4*, *PTGES3*; m6A risk model: *CLDN1*, *ACLY*, *DDX3X*) and integrated models (e.g., intersection-based risk model: *BNIP3*, *BCL2*, *MDM2*, *DDX3X*, *PIK3R1*, *COX5 A*, *VIM*; correlation-based risk model: *CASK*, *SORL1*) have known roles in relevant biological processes. For instance, *NEDD4*'s stability is affected by m6A[38], *PTGES3* is linked to immune responses[39], and *ACLY* is part of a cuproptosis-related signature in cancer[40]. The inclusion of *CASK* and *DDX3X* in our integrated models underscores their potential importance. *CASK*'s link to insulin signaling[41] is highly relevant given insulin resistance in PCOS, while *DDX3X* interacts with lncRNA H19[42], which is dysregulated in PCOS granulosa cells[43]. Further mechanistic studies exploring how these genes contribute to granulosa cell dysfunction and the overall PCOS phenotype are warranted. Our findings regarding granulosa cell gene expression (Fig. 7, S6) partially overlap but also extend those reported by Kõks et al.., who characterized transcriptomic differences between floating and cumulus granulosa cells[44]. While both studies implicate immune signaling and cell-cell interaction pathways, our analysis further integrates m6A methylation and cuproptosis-related signatures, providing additional mechanistic insights into granulosa cell dysfunction in PCOS that were not addressed in the earlier study.

The observed similar GSEA enrichment outcomes and positive correlation between cuproptosis risk score and m6A risk score suggest shared downstream pathways impacted by both cuproptosis and m6A dysregulation

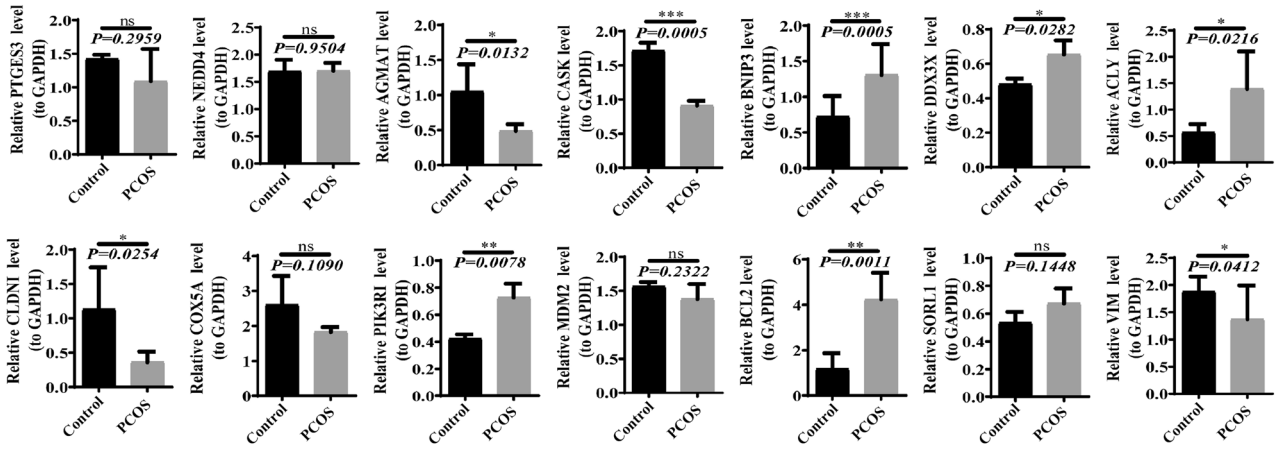

Fig. 8. Comparison of model gene expression levels between the control and PCOS groups via qRT-PCR. Human luteinized granulosa cells were isolated from 5 PCOS patients and 5 controls. Relative mRNA expression levels of selected genes (*AGMAT*, *CASK*, *CLDN1*, *VIM*, *BNIP3*, *DDX3X*, *ACLY*, *PIK3R1*, *BCL2*) normalized to *GAPDH* were compared between groups using the Wilcoxon rank-sum test. Data are expressed as the mean ± SD. $^{*}p < 0.05$, $^{**}p < 0.01$, $^{***}p < 0.001$; ns, non-significant. ($n = 5$ biological replicates per group, each measured in technical triplicate).

in PCOS. This supports the rationale for developing integrated models. PCOS is increasingly recognized as a condition involving chronic low-grade inflammation and immune dysregulation, affecting not only the ovaries but also systemic health[18–20]. Our ssGSEA results align with this, revealing significant differences in immune cell infiltration (e.g., dendritic cells, T cells, MDSCs) between PCOS and control granulosa cell environments (Fig. 5A and B, S5). The correlation of our risk scores with these immune cell populations (Fig. 6C) suggests that cuproptosis and m6A pathways are intertwined with the local immune landscape in PCOS. This resonates with findings by Su et al.. on cuproptosis clusters and immunity in PCOS[34] and Chen et al.. on m6A subtypes and immune infiltration[45]. Our work adds a layer by integrating both pathways and linking them via diagnostic signatures to these immune features.

Growing evidence across diseases supports the role of immune composition in driving microenvironmental remodeling. Ye et al.. have demonstrated that plasma cell-enriched tumors exhibited more active immune landscapes and superior immunotherapy outcomes, highlighting how specific immune cell subsets can restructure tissue homeostasis and responsiveness[46]. Similarly, the iMLGAM framework revealed that immune-infiltrated tumors with low composite risk scores show enhanced cytotoxicity and antigen presentation signatures, defining distinct microenvironmental states that influence therapeutic responsiveness[47]. In addition, elevated systemic immune-inflammation indices (SII) have been associated with shifts toward pro-inflammatory dominance and impaired resolution in mucinous adenocarcinoma, suggesting broader relevance of immune cell composition in remodeling dynamics[48]. Mechanistically, cuproptosis may contribute to microenvironment remodeling by inducing mitochondrial stress, iron-sulfur cluster depletion, and proteotoxic cell death, which can release damage-associated molecular patterns and modulate immune recruitment. m6A RNA methylation, on the other hand, regulates transcriptome plasticity by affecting the stability and translation of immune-modulatory genes, thereby influencing cytokine production, antigen presentation, and stromal interactions. Together, these findings suggest that immune infiltration characteristics, cuproptosis activity, and m6A modifications converge to orchestrate dynamic changes in the PCOS ovarian microenvironment.

Our analysis also revealed intriguing correlations between feature genes and drug sensitivities (Fig. 7, S3, S6). For instance, the link between *ACLY/CLDN1* and Vinblastine sensitivity, and the reported association of high cuproptosis scores with Vinblastine resistance in bladder cancer[49], suggests complex interactions relevant beyond PCOS. The correlation of *CASK* and *CLDN1* with the Wnt inhibitor XAV-939 is particularly interesting. Wnt signaling plays roles in ovarian function and metabolic aspects of PCOS[50]. Given that high m6A risk scores correlate with potential benefits from XAV-939 in renal cancer[51], our finding suggests that XAV-939 warrants investigation in specific PCOS subtypes characterized by alterations in these pathways.

Furthermore, the observed correlations involving *PTGES3* and *FDX1* with AZD-3147[52] hint at synergistic pathway interactions. However, the ABVD chemotherapy regimen containing Vinblastine raises concerns due to its potential impact on ovarian reserve[53,54], especially critical for PCOS patients already facing fertility challenges. These gene-drug correlations, primarily based on cancer cell line data (NCI-60), require cautious interpretation and validation in PCOS-relevant models before clinical translation.

Limitations: While our study offers valuable insights, limitations must be acknowledged. First, the initial DEG analysis relied on merged microarray datasets with relatively small sample sizes for each individual dataset, although merging and batch correction aimed to mitigate this. Second, our findings, particularly the risk scores, require validation in larger, independent, and prospectively collected PCOS cohorts. Third, the immune infiltration analysis is correlative and lacks mechanistic depth; functional studies are needed to elucidate how these pathways modulate immune cells in PCOS. Fourth, the risk prediction models, including their coefficients,

are inherently dependent on the gene expression platform used (primarily microarrays in the discovery phase). Applying these specific coefficients directly to data from other platforms like RNA-seq or qRT-PCR may not be appropriate without recalibration or platform-specific model development. Fifth, the identification of granulosa cells relied heavily on FSHR staining. While standard, confirmation with additional markers could strengthen the findings. Finally, translating these findings into clinically applicable biomarkers, particularly those detectable in peripheral blood, presents both opportunities and challenges. Granulosa cells are not routinely accessible, necessitating the identification of surrogate markers. Prior studies have demonstrated that immune-related genes such as IL18R1, IL7R, and S100A8 are detectable in peripheral blood and can serve as biomarkers in systemic inflammation and pregnancy complications[44,55]. This supports the potential for blood-based transcriptional surrogates of ovarian pathophysiology. However, it remains unclear to what extent the gene expression changes observed in granulosa cells are reflected systemically. Future studies using matched granulosa cell and peripheral blood samples from PCOS patients are essential to assess the diagnostic or prognostic utility of such biomarkers.

Conclusions

In conclusion, our study sheds light on potential synergistic interactions between the m6A modification and cuproptosis pathways in PCOS pathogenesis. We developed integrated diagnostic signatures with high accuracy, linked them to immune microenvironment alterations, and suggested potential avenues for personalized treatment. Despite limitations, these findings provide novel insights and a foundation for future research aimed at improving PCOS diagnosis and management.

Data availability

All data generated or analysed during this study are included in this published article.

Received: 22 July 2024; Accepted: 20 May 2025
Published online: 06 June 2025

References

1. Shukla, A., Rasquin, L. I., Anastasopoulou C.Polycystic Ovarian Syndrome. In: *StatPearls* (StatPearls Publishing, Treasure Island (FL), 2025). Available at https://www.ncbi.nlm.nih.gov/sites/books/NBK459251/.
2. Jain, T. et al. Characterization of polycystic ovary syndrome among Flo app users around the world. *Reprod. Biol. Endocrinol.* **19**, 1–11 (2021).
3. Rudnicka, E. et al. Chronic low grade inflammation in pathogenesis of PCOS. *Int. J. Mol. Sci.* **22**, 3789 (2021).
4. Hoeger, K. M., Dokras, A. & Piltonen, T. Update on PCOS: consequences, challenges, and guiding treatment. *J. Clin. Endocrinol. Metabolism*. **106**, e1071–e1083 (2021).
5. Gibson-Helm, M., Teede, H., Dunaif, A. & Dokras, A. Delayed diagnosis and a lack of information associated with dissatisfaction in women with polycystic ovary syndrome. *J. Clin. Endocrinol. Metabolism*. **102**, 604–612 (2017).
6. Liu, Y. et al. The release of peripheral immune inflammatory cytokines promote an inflammatory cascade in PCOS patients via altering the follicular microenvironment. *Front. Immunol.* **12**, 685724 (2021).
7. Tsvetkov, P. et al. Copper induces cell death by targeting lipoylated TCA cycle proteins. *Science* **375**, 1254–1261 (2022).
8. Victor, V. M. et al. Induction of oxidative stress and human leukocyte/endothelial cell interactions in polycystic ovary syndrome patients with insulin resistance. *J. Clin. Endocrinol. Metabolism*. **96**, 3115–3122 (2011).
9. Dabravolski, S. A. et al. Mitochondrial dysfunction and chronic inflammation in polycystic ovary syndrome. *Int. J. Mol. Sci.* **22**, 3923 (2021).
10. Oc, S., Eraslan, S. & Kirdar, B. Dynamic transcriptional response of Saccharomyces cerevisiae cells to copper. *Sci. Rep.* **10**, 18487 (2020).
11. Sun, Y. et al. High copper levels in follicular fluid affect follicle development in polycystic ovary syndrome patients: Population-based and in vitro studies. *Toxicol. Appl. Pharmcol.* **365**, 101–111 (2019).
12. Li, X., Ma, Z. & Mei, L. Cuproptosis-related gene SLC31A1 is a potential predictor for diagnosis, prognosis and therapeutic response of breast cancer. *Am. J. cancer Res.* **12**, 3561 (2022).
13. Liu, Z. et al. Identification of GLS as a cuproptosis-related diagnosis gene in acute myocardial infarction. *Front. Cardiovasc. Med.* **9**, 1016081 (2022).
14. Deng, L. J. et al. m6A modification: recent advances, anticancer targeted drug discovery and beyond. *Mol. Cancer*. **21**, 1–21 (2022).
15. Zhang, S. et al. Altered m6A modification is involved in up-regulated expression of FOXO3 in luteinized granulosa cells of non-obese polycystic ovary syndrome patients. *J. Cell. Mol. Med.* **24**, 11874–11882 (2020).
16. Zhang, C., Hu, J., Wang, W., Sun, Y. & Sun, K. HMGB1-induced aberrant autophagy contributes to insulin resistance in granulosa cells in PCOS. *FASEB J.* **34**, 9563–9574 (2020).
17. Zhou, L. et al. N6-methyladenosine demethylase FTO induces the dysfunctions of ovarian granulosa cells by upregulating flotillin 2. *Reprod. Sci.* **29**, 1305–1315 (2022).
18. Rostamtabar, M. et al. Pathophysiological roles of chronic low-grade inflammation mediators in polycystic ovary syndrome. *J. Cell. Physiol.* **236**, 824–838 (2021).
19. Moulton, V. R. Sex hormones in acquired immunity and autoimmune disease. *Front. Immunol.* **9**, 2279 (2018).
20. Zhai, Y. & Pang, Y. Systemic and ovarian inflammation in women with polycystic ovary syndrome. *J. Reprod. Immunol.* **151**, 103628 (2022).
21. Yang, L. et al. Ferredoxin 1 is a cuproptosis-key gene responsible for tumor immunity and drug sensitivity: A pan-cancer analysis. *Front. Pharmacol.* **13**, 938134 (2022).
22. Zhao, Y. et al. Identification and validation of novel genes related to immune microenvironment in polycystic ovary syndrome. *Medicine (Baltimore)* **103**, e40229 (2024).
23. Zhu, Y., Tan, J. K. & Goon, J. A. Cuproptosis-and m6A-Related LncRNAs for prognosis of hepatocellular carcinoma. *Biology* **12**, 1101 (2023).
24. Leek, J. T., Johnson, W. E., Parker, H. S., Jaffe, A. E. & Storey, J. D. The Sva package for removing batch effects and other unwanted variation in high-throughput experiments. *Bioinformatics* **28**, 882–883 (2012).
25. Engebretsen, S. & Bohlin, J. Statistical predictions with Glmnet. *Clin. Epigenetics*. **11**, 123 (2019).
26. Robin, X. et al. pROC: an open-source package for R and S + to analyze and compare ROC curves. *BMC Bioinform.* **12**, 1–8 (2011).
27. Yu, G., Wang, L. G., Han, Y. & He, Q. Y. ClusterProfiler: an R package for comparing biological themes among gene clusters. *Omics: J. Integr. Biology*. **16**, 284–287 (2012).

28. Zhang, Z. & Kattan, M. W. Drawing nomograms with R: applications to categorical outcome and survival data. *Annals Translational Med.* **5**, 211 (2017).
29. Li, H. et al. Decision curve analysis to identify optimal candidates of liver resection for intermediate-stage hepatocellular carcinoma with hepatitis B cirrhosis: A cohort study. *Medicine* **101**, e31325 (2022).
30. Charoentong, P. et al. Pan-cancer Immunogenomic analyses reveal genotype-immunophenotype relationships and predictors of response to checkpoint Blockade. *Cell. Rep.* **18**, 248–262 (2017).
31. Hanzelmann, S., Castelo, R. & Guinney, J. GSVA: gene set variation analysis for microarray and RNA-seq data. *BMC Bioinform.* **14**, 7 (2013).
32. Group, R. E. A. S. P. C. W. Revised 2003 consensus on diagnostic criteria and long-term health risks related to polycystic ovary syndrome (PCOS). *Human reproduction*. 19, 41–47 (2004).
33. Panel, E. Chinese guideline for diagnosis and management of polycystic ovary syndrome. *Zhonghua Fu Chan Ke Za Zhi*. **53**, 2–6 (2018).
34. Su, Z., Su, W., Li, C., Ding, P. & Wang, Y. Identification and immune features of cuproptosis-related molecular clusters in polycystic ovary syndrome. *Sci. Rep.* **13**, 980 (2023).
35. Zhou, S., Hua, R. & Quan, S. N6-methyladenosine regulator-mediated methylation modification patterns and immune infiltration characterization in polycystic ovary syndrome (PCOS). *J. Ovarian Res.* **16**, 1–15 (2023).
36. Qin, H. et al. Comprehensive analysis of cuproptosis-related prognostic gene signature and tumor immune microenvironment in HCC. *Front. Genet.* **14**, 1094793 (2023).
37. Yu, H. et al. A signature of cuproptosis-related lncRNAs predicts prognosis and provides basis for future anti-tumor drug development in breast cancer. *Transl. Cancer Res.* **12**, 1392–1410 (2023).
38. Lin, K. et al., *FTO Deubiquitinated by USP7 Influenced NEDD4 mRNA Stability Enhancing the Chemoresistance of Pancreatic Cancer to Gemcitabine by Promoting Cell Proliferation and Regulating PTEN/PI3K/AKT Pathway.* Available at SSRN 4258954. (2022).
39. Yu, Z., He, Q. & Xu, G. Effect of N6-methyladenosine (m6A) regulator-related immunogenes on the prognosis and immune microenvironment of breast cancer. *Translational Cancer Res.* **11**, 4303 (2022).
40. Hu, Y. et al. Construction of a Cuproptosis-Related Gene Signature for Predicting Prognosis in Gastric Cancer. *Biochem. Genet.* **62**, 40–58 (2024).
41. Wang, Y. et al. Proteomic analysis reveals novel molecules involved in insulin signaling pathway. *J. Proteome Res.* **5**, 846–855 (2006).
42. Ma, Y. et al. Long noncoding RNA H19 inhibits the growth and invasion of trophoblasts by inactivating Wnt/beta-catenin signaling via downregulation of DDX3X. *Int. J. Clin. Exp. Pathol.* **10**, 6560–6567 (2017).
43. Li, L., Wei, J., Hei, J., Ren, Y. & Li, H. Long non-coding RNA H19 regulates proliferation of ovarian granulosa cells via STAT3 in polycystic ovarian syndrome. *Archives Med. Science: AMS.* **17**, 785 (2021).
44. Kõks, S. et al. The differential transcriptome and ontology profiles of floating and cumulus granulosa cells in stimulated human antral follicles. *Mol. Hum. Reprod.* **16**, 229–240 (2010).
45. Chen, J., Fang, Y., Xu, Y. & Sun, H. Role of m6A modification in female infertility and reproductive system diseases. *Int. J. Biol. Sci.* **18**, 3592 (2022).
46. Ye, B. et al. Navigating the immune landscape with plasma cells: A pan-cancer signature for precision immunotherapy. *BioFactors* **51**, e2142 (2025).
47. Ye, B. et al., *iMLGAM: Integrated Machine Learning and Genetic Algorithm-driven Multiomics analysis for pan-cancer immunotherapy response prediction. iMeta. e70011* (2025).
48. Sun, W. et al. Systemic immune-inflammation index predicts survival in patients with resected lung invasive mucinous adenocarcinoma. *Translational Oncol.* **40**, 101865 (2024).
49. Song, Q., Zhou, R., Shu, F. & Fu, W. Cuproptosis scoring system to predict the clinical outcome and immune response in bladder cancer. *Front. Immunol.* **13**, 958368 (2022).
50. Luan, Y., Zhang, L., Peng, Y., Li, Y. & Liu, R. x.& Yin, C.-h. Immune regulation in polycystic ovary syndrome. *Clin. Chim. Acta*. **531**, 265–272 (2022).
51. Fan, G. et al. Genes associated with N6-methyladenosine regulators provide insight into the prognosis and immune response to renal clear cell carcinoma. *Environ. Toxicol.* **39**, 626–642 (2024).
52. Zhang, C. et al. Pan-cancer analyses confirmed the cuproptosis-related gene FDX1 as an immunotherapy predictor and prognostic biomarker. *Front. Genet.* **13**, 923737 (2022).
53. Yubing, L., Xinmei, L., Xiaocan, L. & Chian, R. Effect of Adriamycin, bleomycin, vinblastine and Dacarbazine (ABVD) treatment on female mice reproductive function. *Fertil. Steril.* **112**, e246 (2019).
54. McLaughlin, M., Kelsey, T. W., Wallace, W., Anderson, R. & Telfer, E. Non-growing follicle density is increased following Adriamycin, bleomycin, vinblastine and Dacarbazine (ABVD) chemotherapy in the adult human ovary. *Hum. Reprod.* **32**, 165–174 (2017).
55. Rull, K. et al. Increased placental expression and maternal serum levels of apoptosis-inducing TRAIL in recurrent miscarriage. *Placenta* **34**, 141–148 (2013).

Author contributions

Yang Liu and Jia Bie carried out the studies, participated in collecting data, and drafted the manuscript. Yujie Gengxiao and Yanzhi Wu performed the statistical analysis and participated in its design. Yang Liu, Yan Li and Xi Hu participated in acquisition, analysis, or interpretation of data and draft the manuscript. All authors read and approved the final manuscript.

Funding

The study was supported by the Famous Doctor Project of Xingdian Talent Support Program in Yunnan Province [XDYC-MY-2022-0057]; Academic Leaders and Candidates of Kunming Medical University - "Riding the Wind" Talent Training Program [2023 (108)]; External Cooperation Research Project of the Second Affiliated Hospital of Kunming Medical University - Mechanism of histone lactate regulation of METTL3 in PCOS affecting the proliferation of ovarian granulosus cells [2022 dwhz03].

Declarations

Competing interests

The authors declare no competing interests.

Ethics approval and consent to participate

The study was approved by the Ethics Committee of the Second Affiliated Hospital of Kunming Medical University (No.2023 – 238). All participants provided written informed consent. We confirm that all methods were performed in accordance with the relevant guidelines. All procedures were performed in accordance with the ethical standards laid down in the 1964 Declaration of Helsinki and its later amendments.

Additional information

Supplementary Information The online version contains supplementary material available at https://doi.org/10.1038/s41598-025-03396-8.

Correspondence and requests for materials should be addressed to Y.L. or J.B.

Reprints and permissions information is available at www.nature.com/reprints.

Publisher's note Springer Nature remains neutral with regard to jurisdictional claims in published maps and institutional affiliations.

Open Access This article is licensed under a Creative Commons Attribution-NonCommercial-NoDerivatives 4.0 International License, which permits any non-commercial use, sharing, distribution and reproduction in any medium or format, as long as you give appropriate credit to the original author(s) and the source, provide a link to the Creative Commons licence, and indicate if you modified the licensed material. You do not have permission under this licence to share adapted material derived from this article or parts of it. The images or other third party material in this article are included in the article's Creative Commons licence, unless indicated otherwise in a credit line to the material. If material is not included in the article's Creative Commons licence and your intended use is not permitted by statutory regulation or exceeds the permitted use, you will need to obtain permission directly from the copyright holder. To view a copy of this licence, visit http://creativecommons.org/licenses/by-nc-nd/4.0/.

© The Author(s) 2025